REMOTE SENS. ENVIRON. 48:159–171 (1994)

Comparisons of Remotely Sensed and Model-Simulated Soil Moisture over a Heterogeneous Watershed

D.-S. Lin[*], *E. F. Wood*,[*] *P. A. Troch*,[†] *M. Mancini*,[‡] *and T. J. Jackson*[§]

Soil moisture estimates from a distributed hydrologic model and two microwave airborne sensors (Push Broom Microwave Radiometer and Synthetic Aperture Radar) are compared with ground measurements on two different scales, using data collected during a field experiment over a 7.4-km² heterogeneous watershed located in central Pennsylvania. It is found that both microwave sensors and the hydrologic model successfully reflect the temporal variation of soil moisture. Watershed-averaged soil moistures estimated by the microwave sensors are in good agreement with ground measurements. The hydrologic model initialized by streamflow records yields estimates that are wetter than observations. The preliminary test of utilizing remotely sensed information as a feedback to correct the initial state of the hydrologic model shows promising results.

INTRODUCTION

Soil moisture can be defined as the storage of precipitation within a shallow layer of the earth that is generally limited to the aeration zone. Despite the insignificant amount of water compared to the global water budget, soil moisture governs the runoff generation processes and provides the linkage between the hydrologic cycle and the energy cycle through evapotranspiration. It is, therefore, an important variable in many hydrologic and agricultural investigations. Recent studies with the general circulation models (GCMs) using active land surface parameterization have shown that strong feedbacks existed between the soil moisture anomalies and climate (see Wood, 1991).

As a result of the inhomogeneity of soil properties, vegetation, and precipitation, soil moisture is highly variable both spatially and temporally. The measurement of soil moisture is traditionally conducted on a point basis. Spatial soil moisture distribution is often obtained through interpolation of point measurement. Acquiring a spatial soil moisture map over a heterogeneous area through conventional techniques can be expensive and time-consuming.

Recent advances in microwave remote sensing have demonstrated the ability to measure soil moisture in the surface layer of a depth of approximately 5 cm under a variety of topographic and land cover conditions (Engman, 1990). Despite the promising perspective of the remote sensing technique, its application to agricultural and hydrologic sciences has been hampered by several difficulties. First, existing hydrologic models are conventionally formulated on point processes. These models are not capable of using the remotely sensed data as direct input. In addition, the algorithms that are currently used to extract soil moisture from the microwave measurements have limited ranges of validity and are subject to further verifications. A better understanding of these problems will be needed in order to efficiently utilize the microwave remotely sensed information.

This article compares remotely sensed and model simulated soil moistures with ground observations over a heterogeneous watershed, using the data collected

[*]Department of Civil Engineering and Operations Research, Princeton University
[†]Laboratory of Hydrology and Water Management, Ghent University, Ghent, Belgium
[‡]DIIAR, Politecnico di Milano, Milano, Italy
[§]USDA / ARS Hydrology Laboratory, Beltsville

Address correspondence to Dah-Syang Lin, Dept. of Civil Engineering, Princeton Univ., Princeton, NJ 08544.
Received 21 October 1992; revised 18 September 1993.

0034-4257 / 94 / $7.00

655 Avenue of the Americas, New York, NY 10010

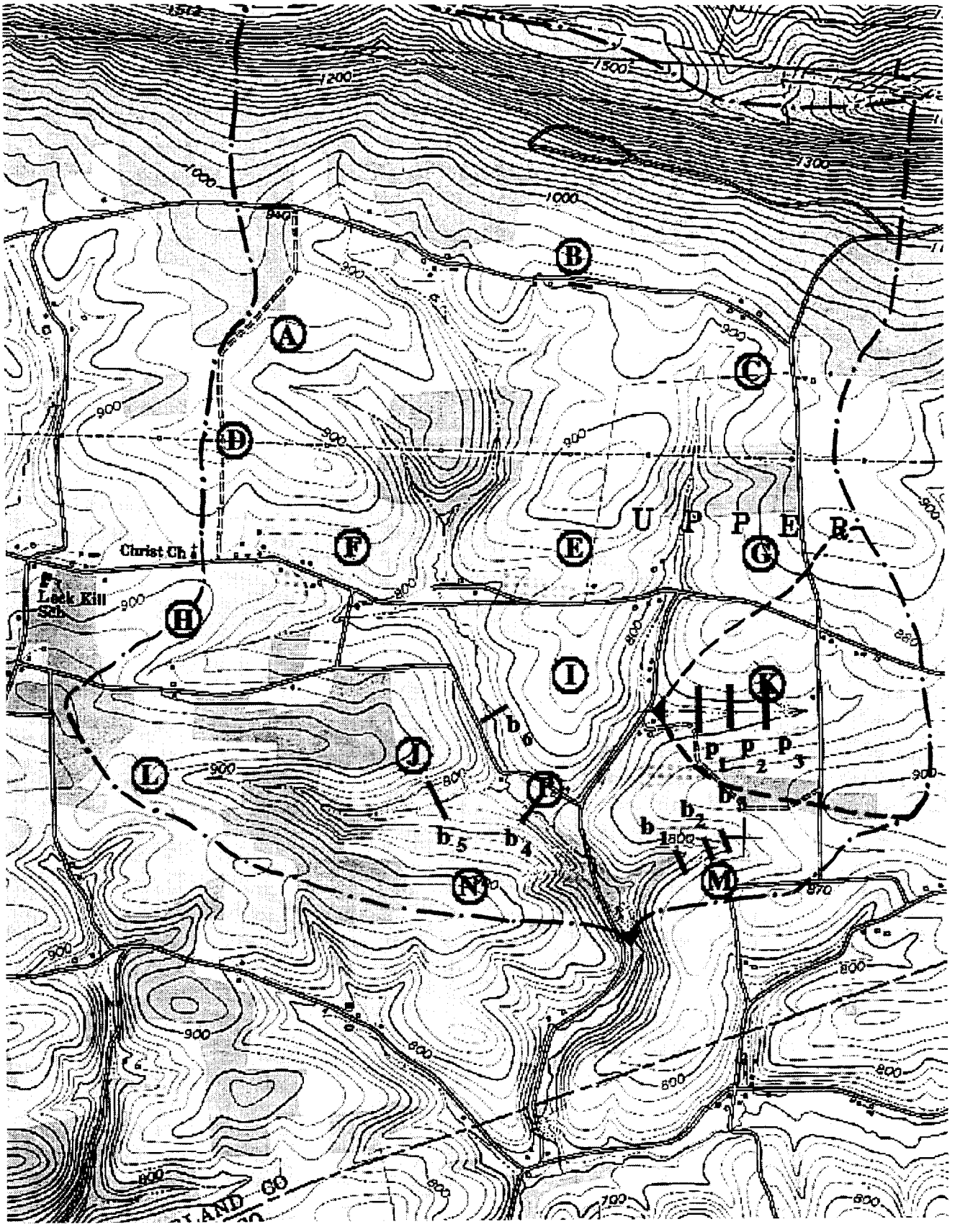

Figure 1. topography map for MAC-HYDRO'90 test site. Circled letters represent the location of the raingages. b_1–b_6 and p_1–p_3 are transects along which soil samples were taken. The 7.4-km^2 research watershed is outlined by the dotted line. Dash line is used to depict the WD38 subcatchment. The solid triangles indicate the location of the weirs.

in a multisensor aircraft campaign (MAC-HYDRO'90) designed to study the sensors' performances and their application to hydrologic applications. Both active and passive microwave sensors have been flown during the MAC-HYDRO'90 experiment. The objective of this article is, through intercomparisons, to examine the restrictions of the current microwave remote sensing techniques used in soil moisture estimation. We will explore the problems that one is likely to encounter when attempting to incorporate the remotely sensed data into a modeling framework.

An overview of the MAC-HYDRO'90 experiment and some pertinent information are given in the next section. In the third section, features of the two microwave sensors and the hydrologic model used in the simulation are presented, along with the methods are analysis. Results of intercomparisons are presented and discussed in the fourth section, followed by the conclusions.

MAC-HYDRO'90 EXPERIMENT

Site Description

MAC-HYDRO'90 was conducted over a portion of the Mahantango Creek which is a 7.4-km^2 research watershed operated by the Northeast Watershed Research Center of the U.S. Department of Agriculture (USDA) Agricultural Research Service (ARS) in central Pennsylvania (see Fig. 1). The average annual precipitation and evapotranspiration for the watershed are 1128 mm and 479 mm per year, respectively. The soils within this watershed are primarily silt loams and loams, and contain approximately 0.5–2.0% organic carbon. Rock fragments are present in the surface layer in some soils.

The intensive study area includes a subwatershed (WD38) of about 50 ha on the eastern portion of Mahantango Creek. The WD38 subwatershed contains a mixture of land uses (corn, wheat, oat, pasture, and hay) and is bounded on the south by forest. Vegetation and soil moisture samples were also taken from several large agricultural fields located outside the main watershed (see Fig. 2).

Weather Conditions

The weather conditions during the experiment were dry initially. No rain was recorded during the preceding 5 days, resulting in uniformly dry soil conditions. After the first flight (10 July 1990), there was an approximately 52 mm of precipitation over a 4-day period, followed by a strong drydown. These conditions generated a wide range of soil moisture conditions, which provide an excellent test ground for the remote sensing techniques. The rainfall record and the dates of data collections are outlined in Table 1.

DATA AND METHODS OF ANALYSIS

Ground Measurements

Soil samples were taken during the time of the overflights. For large agricultural fields, samples were taken on a grid to provide a field-averaged soil moisture value. In addition, samples were collected along transects which were aligned at right angles to the streams. The

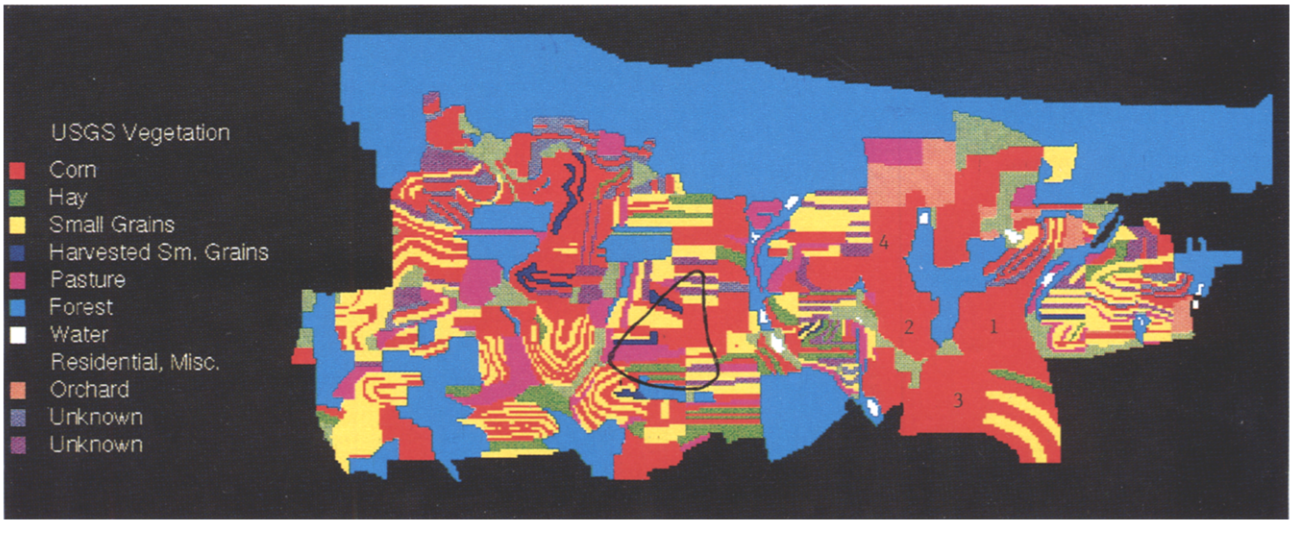

Figure 2. Land cover map for the studied area derived from aerial photographs and field observations. The four large corn fields are indicated by the Arabic numbers.

Table 1. MAC-HYDRO'90 Data Collection and Rainfall Record

Date	*Rainfall Accumulation (mm)*	*PBMR*	*SAR*	*Ground Data*
10 July	0	Yes	Yes	Yes
13 July	39	No	Yes	Yes
15 July	52	Yes	Yes[a]	Yes
17 July	52	Yes	Yes[a]	Yes
18 July	52	Yes	No	Yes
19 July	52	Yes	No	Yes
20 July	52	No	No	Yes

[a] Also high-resolution data.

location of the nine transects can be seen in Figure 1. To provide a vertical soil moisture profile, soil samples were taken at two depths, 0–5 cm and 5–10 cm. Each sample contains approximately 125 cm^3 of soils in volume.

Land cover information was compiled for the entire studied area, shown in Figure 2. Ten categories are used to classify different types of land cover. Vegetation configurations (height, density, dimension, biomass, and orientation distribution) were gathered from representative agricultural fields to help in studying the interactions between microwaves and vagetation canopies.

Rainfall records were collected from a network of 15 tipping-bucket raingages deployed over the main watershed (see Fig. 1). A micrometeorological station located near the raingage H was used to collect meteorological data. Figure 3a shows the time series of the areal average precipitation computed from the 15-min rainfall data. Figure 3b shows the potential evaporation calculated using the Priestley–Taylor method from observed net radiation at a sampling interval of 30 min.

A detailed soil map was assembled from the literatures (Rogowski et al., 1974; Loague and Freeze, 1985). Fifteen soil types can be identified within the studied watershed. The hydraulic properties of these soils are listed in Table 2. Topography of the area is depicted by the USGS 7.5-min digital elevation model (DEM) data. Resolution of the 7.5-min DEM is 30 m × 30 m.

Figure 3. Time series of a) the areal average precipitation and b) the potential evaporation (ETP) during the period from 9 to 20 July 1990.

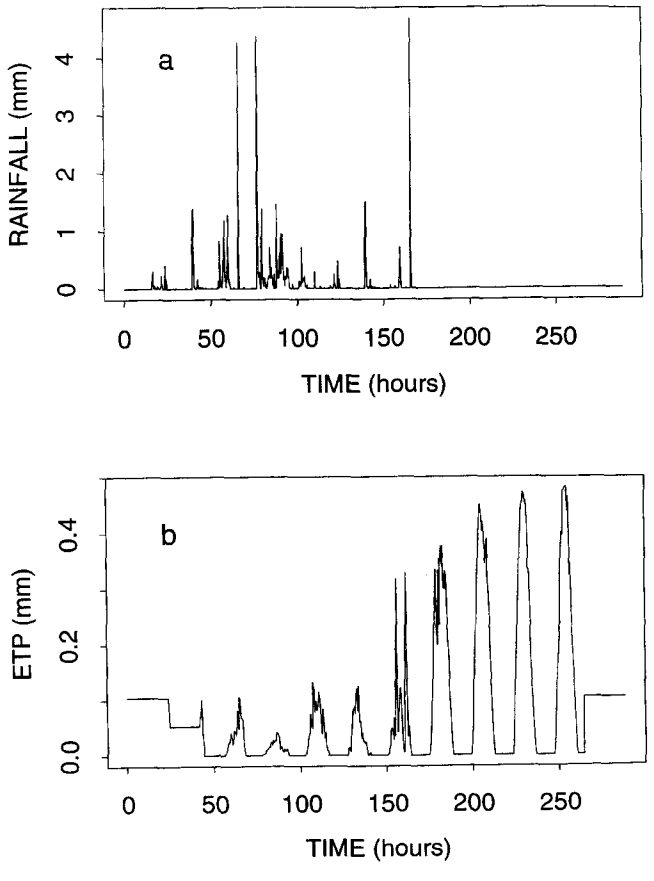

Passive Microwave Radiometer

The passive microwave sensor used in MAC-HYDRO'90 was the push broom microwave radiometer (PBMR). The PBMR operates at L-band ($f = 1.42$ GHz) and has four horizontally polarized beams pointing at $\pm 8°$ and $\pm 24°$ from nadir. The cross-track resolution of the PBMR is approximately 90 m during MAC-HYDRO'90. Schmugge et al. (1988) give a detailed description of the instrument.

Data collected from the PBMR were processed using the procedures that have been successfully employed in previous experiments (Schmugge et al., 1992). The final product consists of the averaged brightness temperatures, stored in a grid system. Notice that the pixel resolution of the PBMR brightnes temperature map does not necessaryily correspond to the intrinsic resolution of the instrument. For MAC-HYDRO'90, the pixel resolution is 20 m × 20 m. Errors caused by aircraft motion (e.g., pitch, roll, and yaw) are not taken into consideration.

To extract the soil moisture from the PBMR brightness temperature map, we adopt the method described in Jackson and Schmugge (1991). The vegetation water content and the optical thickness are first estimated for each land cover type. These information are used to calculate the watershed averaged optical thickness. Then, using the following relationships, the relative soil dielectric constant ε_r is inferred:

$$T_B = [1 - R_H^2 \cdot \exp(-2\bar{\tau} \sec \theta)] \cdot T_v, \quad (1)$$

$$R_H^2 = \left| \frac{\varepsilon_r - 1}{[\cos \theta + \sqrt{\varepsilon_r - \sin^2 \theta}]^2} \right|^2, \quad (2)$$

where T_B and T_v are the averaged brightness temperature and vegetation physical temperature, respectively. T_v is assumed to be equal to the surface soil tempera-

Table 2. Hydraulic Properties of Various Soils within the Studied Watershed

Soil Name	*Soil Texture*	*Saturation Conductivity (mm/h)*	*Residual Soil Moisture*	*van Genuchten parameter, n*
Albrights	Silt loam	0.036	0.015	1.29
Alvira	Silt loam	0.036	0.015	1.29
Basher	Silt loam	0.036	0.015	1.29
Berks	Silt loam	0.073	0.015	1.29
Calvin	Silt loam	0.057	0.015	1.29
Conyngham	Silt loam	0.036	0.015	1.29
Dekalb	Sandy loam	0.090	0.041	1.38
Hartleton	Silt loam	0.057	0.015	1.29
Klinesvil	Silt loam	0.090	0.015	1.29
Laidig	Gravel loam	0.090	0.027	1.25
Leck Kill	Silt loam	0.057	0.015	1.29
Meckesville	Loam	0.036	0.015	1.29
Meckesville	Stony loam	0.090	0.015	1.29
Shelmadine	Silt loam	0.036	0.015	1.29
Weickert	Silt loam	0.073	0.015	1.29

ture. R_H^2 is the H-polarized reflectivity of the air-soil interface, $\bar{\tau}$ is the averaged optical thickness, and θ is the look angle for the PBMR, which is approximately equal to 10°.

Finally, the semiempirical dielectric mixing model proposed by Dobson et al. (1985) is used in this study to invert the volumetric soil moisture content.

Synthetic Aperture Radar

Aircraft radar data were acquired over the Mahantango Creek using the Jet Propulsion Laboratory multipolarization imaging radar (JPL AIRSAR) in three frequencies (f = 0.44 GHz, 1.25 GHz, and 5.33 GHz). For the configurations of the instrument, refer to Held et al. (1988). Three flight lines were flown each day with the objective of obtaining multiple incidence angles (20°, 30°, and 45°) of the target area (76°35′W, 40°43′N). The slant range resolution of the processed images is 6.662 m under the normal mode. On 15 and 17 July 1990, high resolution data with a 3.331 m slant range pixel size were also available. The azimuth pixel resolution remains to be 12.1 m for both modes.

The AIRSAR imagery were calibrated for phase, cross-talk, channel imbalance, and absolute power using trihedral corner reflectors. At least one corner reflector was available for calibration in every scene. The underlying theories and algorithms for signal calibrations are presented in van Zyl et al. (1990). Recent measurements with the AIRSAR over the California desert have achieved a calibration accuracy within 1 dB for like-polarized signals (Durden et al., 1991).

Hydrologic Model

The hydrologic model employed in this study was developed by Paniconi and Wood (1992). This model predicts patterns of soil moisture by solving the three-dimensional Richards equation. Richards equation with pressure head ψ as the dependent variable can be written as

$$S(\psi)\frac{\partial \psi}{\partial \psi} = \nabla \cdot [K_s K_r(\psi) \nabla (\psi + z)], \tag{3}$$

where t is time and z is the vertical coordinate, positive upward. The hydraulic conductivity is expressed as a product of the conductivity at saturation, K_s, and the relative conductivity K_r. $S(\psi)$ represents the specific moisture capacity.

An extension of the van Genuchten characteristic equations (van Genuchten and Nielsen, 1985) is used to describe the relationships of volumetric moisture content M_v with the related soil properties such as $S(\psi)$, hydraulic conductivity, and pressure head. The saturated hydraulic conductivity is assumed to decline exponentially with depth, an assumption consistent with field observations (Beven, 1983; Paniconi and Wood, 1992). Hysteresis effects on moisture redistribution are not taken into account in this version of the model. Evaporation and infiltration are controlled either by the atmospheric conditions or by the soil conditions, depending on the demand and supply capability.

The initial condition is determined using the procedure proposed by Troch et al. (1992), which is based on the Boussinesq's equation and uses streamflow data at the outlet of the watershed. The lower and lateral boundaries are assumed to be impervious. The depth of the lower boundary is fixed at 5 m below the soil surface. Given the initial and boundary conditions, the system is solved by a finite element method described in Paniconi et al. (1991) and Paniconi and Wood (1992) for the 11-day duration of the experiment (from 9 to 20 July). Solutions include not only the surface soil moisture contents but also the vertical moisture profile of

the unsaturated zone for each pixel within the computational domain.

Image Integration

To allow intercomparisons of soil moisture estimates from various sources, all imagery are registered with reference to the DEM. A six-parameter affine transformation is used in the process. This transformation can be expressed in the following form:

$$x' = Ax + By + C,$$
$$y' = Dx + Ey + F, \quad (4)$$

where x' and y' are the calculated x- and y-coordinates of the pixel on the DEM and x and y are the column and row numbers of a pixel in the image. A–E are coefficients to be determined from the tie points between the image and the DEM.

Georeferenced images are then resampled to the resolution of the DEM using a bilinear interpolation scheme. The final product consists of several layers of meshes, each one containing different information such as land cover, local incidence angle, soil type, and averaged microwave measurements from the PBMR and the SAR.

The accuracy of the resulting data depends on several factors: how well the tie points are located, the number of tie points used, the interpolation scheme, and the accuracy of the aircraft navigation systems. It should be pointed out that ground locations of the SAR pixels can be directly calculated from the geometry of the radar system, which is given in the header of the imagery, and the DEM data. This approach is, however, not exercised because the watershed under study is probably too small for this approach to yield accurate results. In general, the registration procedure used in this study works fairly well except for the cases where the SAR images were taken from small incidence angles. Because the target area is contracted in the small incidence angle SAR imagery, selection of the tie points becomes very difficult. Due to the large uncertainties associated with the resulting data, the 20° and 30° SAR imagery will not be used in the subsequent analysis.

The above procedure has also been used to extrapolate the DME data on top of the SAR imagery. The advantage of doing so is that the fine resolution of the SAR can be preserved. Figure 4 displays a DEM-registered high resolution L-band ($f = 1.25$ GHz) SAR image. This HH-polarized SAR image was taken on 15 July 1990 from a 45° incidence angle. A comparison between the figure and the topographic map (Fig. 1) indicates that the registration procedure is highly reliable.

Figure 4. A high resolution L-band HH-polarized DEM-registered SAR image taken on 15 July 1990 from a 45° look angle.

RESULTS AND DISCUSSION

In this section, we present results of soil moisture intercomparisons along transects and over the WD38 watershed. Before the comparisons are performed, the data processing procedures presented in the preceding section are tested on several large agricultural fields to evaluate their performances. Data collected over these agricultural fields are also used in developing empirical inversion algorithms for the SAR.

Large Agricultural Field Comparisons

Four corn fields located east of the main watershed are selected for verification sites (see Fig. 2). These corn fields are the largest accessible agricultural fields in the area. The corn stood 90 cm in height during the experiment and contained approximately 2 kg/m^2 of water. Density of corn ranged from 4.88 to 6.74 plants per m^2. The averaged soil bulk density was 0.74 g/cm^3 with a standard deviation of 0.25 g/cm^3.

Figure 5 plots the temporal variations of the PBMR brightness temperatures and the L-band HH-polarized backscattering coefficients of the SAR averaged over corn fields 1 and 2 during the course of the experiment. Volumetric soil moisture contents from ground measurements are also displayed for comparisons. It is found that the brightness temperatures measured by the PBMR decrease with increasing soil wetness. Meanwhile, stronger SAR backscattering signals are observed on wet days. In general, both instruments have reflected the current temporal variations of soil moisture on these large corn fields.

We next compare, in Figure 6, the PBMR estimated soil moistures with the ground measurements over the corn fields. As shown in the figure, the PBMR soil moisture estimation procedure functions pretty well. Notice that each observed value in the figure represent

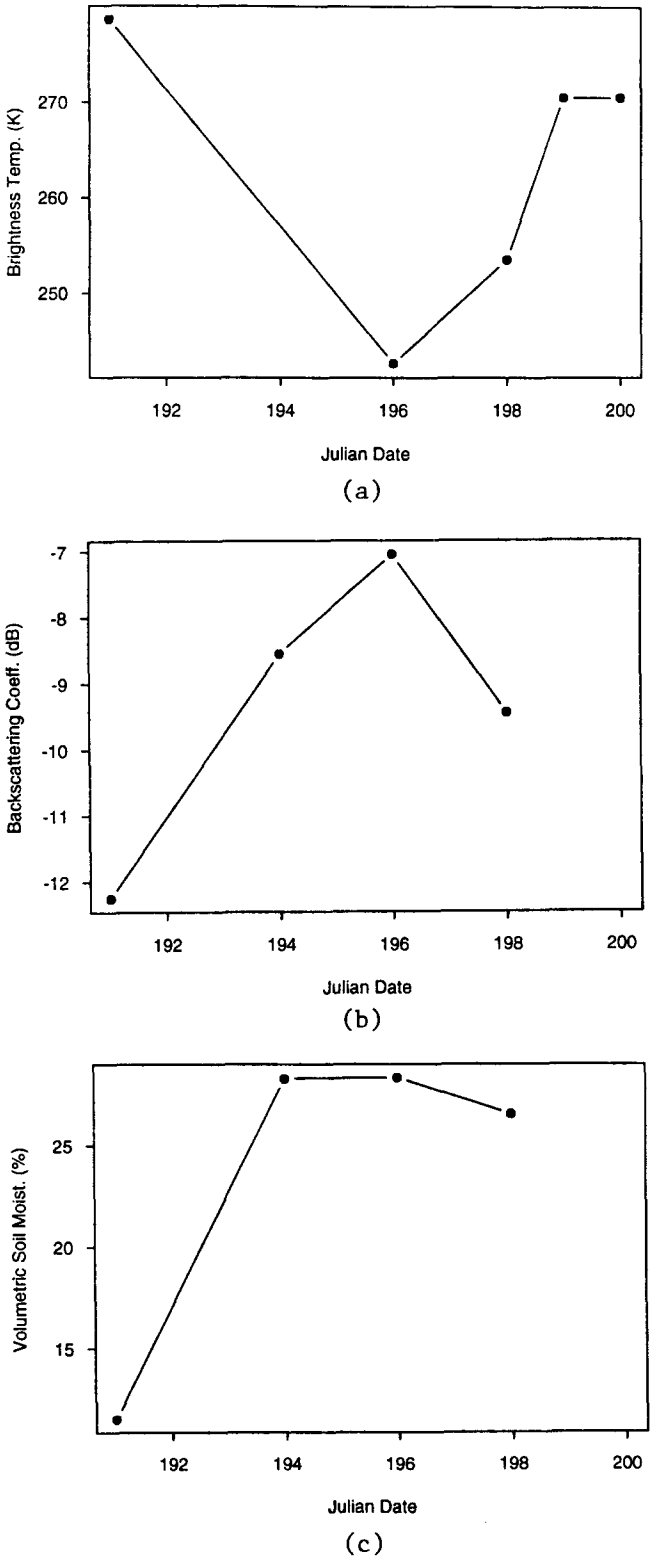

Figure 5. Temporal variations of a) the PBMR brightness temperatures, b) the L-band HH-polarized SAR backscattering coefficients, and c) the volumetric soil moistures averaged over corn fields 1 and 2 during the course of MAC-HYDRO'90.

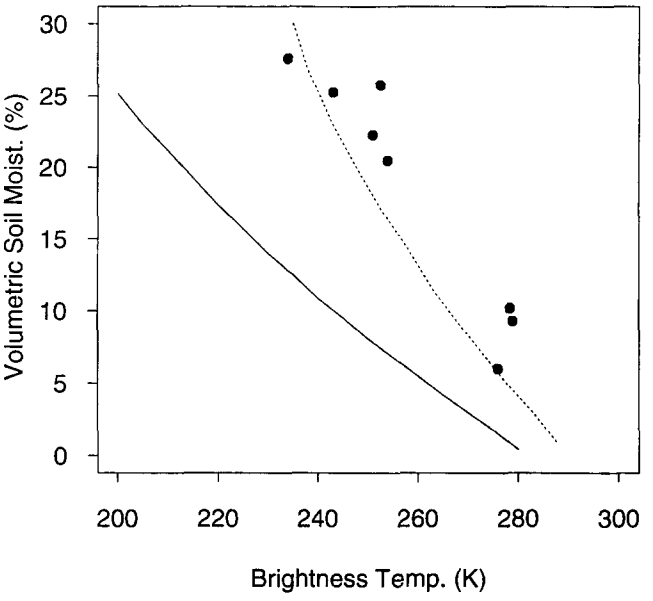

Figure 6. Observed and predicted soil moistures and the PBMR brightness temperature data for the corn field verification sites. Solid line represents bare soil surface. Dash line represents vegetation water content of 2 kg / m^2. Ground observations are represented by dots.

an average of at least 16 soil samples collected in the fields. These results provide us a basis for applying the same PBMR estimation algorithm to the entire watershed.

Soil moisture inversion algorithms for the SAR have been the subject of research for some time. Most existing algorithms are developed for bare soil surfaces (e.g., Soares et al., 1991; Oh et al., 1992) and are based on data measured by different instruments (e.g., truck-mounted scatterometer). Pultz et al. (1990) have presented an empirical relationship that can be used for quantitative soil moisture extraction from the airborne SAR data over wheat and canola fields, developed using concurrent ground measurements and data acquired from a C-band HH-polarized SAR over a test site in Canada. However, as pointed out by the authors, this relationship may be site-specific and is only effective for crops at the emergent stage. Since there is no existing algorithm that can be readily applied to the MAC-HYDRO'90 test site, it is decided to develop a new set of empirical relationships for our purposes. In doing so, SAR backscatters of various polarizations from four corn fields, two oat fields, and a number of pasture areas are extracted from the images and averaged over the areas. The characteristics of these fields are summarized in Table 3. The extracted SAR data are in turn regressed with the corresponding 0–5 cm volumetric soil moisture measurements using a simple linear regression model. Table 4 presents the results of the regression analysis. It appears that, evaluated from the correlation coefficients r, no particular combination of frequency and polarization has yielded a decisive edge over others.

Table 3. Characteristics of the Fields Used in Developing the SAR Inversion Algorithms

Land Cover	*Range of Incidence Angle (°)*	*Range of Soil Moisture (%)*	*Average Height (cm)*
Corn	36–46	6–32	90
Oat	38–42	8–28	75
Pasture	35–39	14–40	25

The P-band radar data are not included in the analysis because, during MAC-HYDRO'90, their signal-to-noise ratios are often so low in the neighborhood of the corner reflectors that accurate calibration of the signals cannot be guaranteed.

There are several problems needed to be clarified before one can apply the above relationships for the soil moisture retrieval purposes. First, it should be pointed out that the above relationships are based on a rather limited number of samples and on the assumption that radar signals vary linearly with soil wetness within the range of soil moisture conditions considered. Second, due to the weather conditions during the experiment, the values of the volumetric soil moisture content are clustered to the two extremes, thus providing limited information about the transition period. As a result, the predictive power of the developed relationships should be carefully evaluated. Finally, it is well known that, in addition to soil moisture, SAR signals are also sensitive to a number of land-surface parameters such as vegetation properties and topography. By neglecting these land-surface parameters, we have implicitly narrowed the range of validity for the developed relationships, which can be approximated by the conditions listed in Table 3. To apply these relationships to the whole watershed, one needs to first check whether the vegetation properties and the local incidence angles of the areas are within the range of validity of these relationships.

Transect Comparisons

For comparisons between the remotely sensed and model simulated soil moistures along transects, we focus our attention on the area between the transects P_1 and P_2 (see Fig. 1). Transects P_1 and P_2 were aligned perpendicularly to a small stream that flows in an east-to-west direction. The distance between these two transects is approximately 60 m. Within this area, there are three different types of land cover (corn, pasture, and wheat stubble) extended like stripes parallel to the stream and to the flight track of the aircraft. The particular configuration of the selected area allows us to include more pixels to perform a statistically meaningful comparison.

Figures 7a and 7b compare the soil moisture patterns reflected by various sources along transects P_1 and P_2 for 10 and 17 July 1990, respectively. Pixels situated within the selected area are averaged horizontally (i.e., parallel to the stream). Since the units of various data are different, measurements from different sources are normalized with respect to their arithmetic means to allow for intercomparisons. The PBMR data are excluded from this comparison because the current georeferencing technique is insufficient to accurately locate the measurements on the transect scale. It can be seen from the figure that the SAR successfully picks up the soil moisture patterns measured by the ground samples, showing the high soil wetness in the proximity of the stream and low soil moisture content over the corn field on both the dry and wet days.

Table 4. Results of Linear Regression Analysis

Canopy	*Band*	*Polarization*	*Slope*	*Intercept*	*r*
Corn	C	HH	4.374	55.670	0.730
	C	VV	4.915	64.464	0.837
	C	HV	7.097	131.298	0.863
	L	HH	2.625	50.986	0.783
	L	VV	0.979	32.666	0.525
	L	HV	3.329	95.786	0.827
Oat	C	HH	3.403	48.377	0.831
	C	VV	3.298	61.623	0.894
	C	HV	3.411	82.146	0.657
	L	HH	3.672	89.835	0.805
	L	VV	3.481	87.214	0.908
	L	HV	1.800	74.185	0.590
Pasture	C	HH	0.552	39.933	0.821
	C	VV	1.002	48.379	0.633
	C	HV	9.559	199.410	0.884
	L	HH	4.792	92.029	0.642
	L	VV	5.161	95.083	0.909
	L	HV	3.894	130.767	0.471

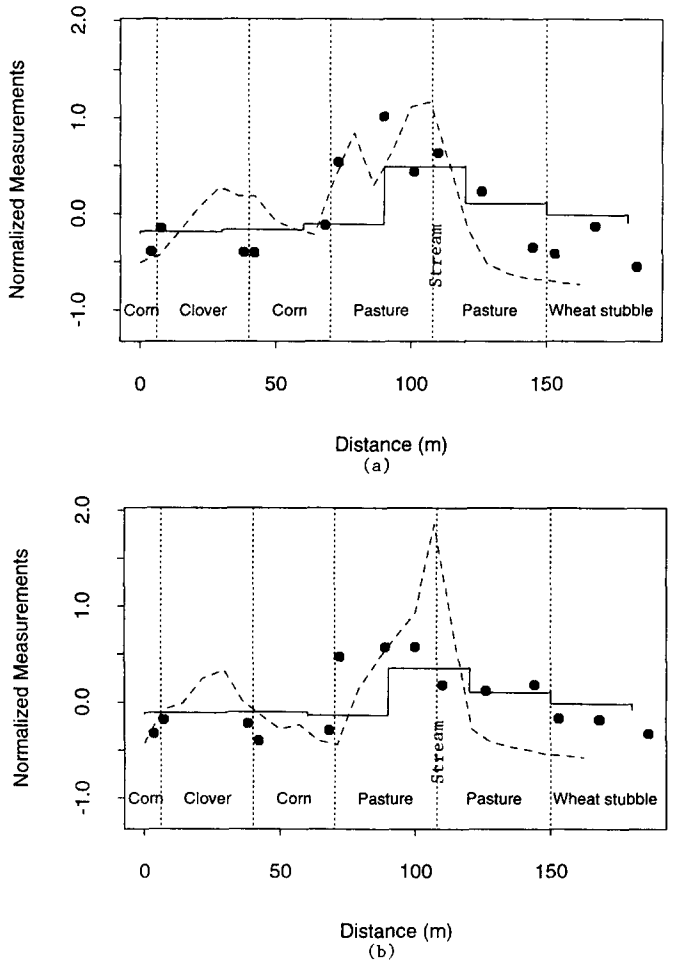

Figure 7. Soil moisture patterns reflected by various sources along transects P_1 and P_2 on a) 10 July and b) 17 July 1990. Dots stand for ground measurements. The SAR signals are represented by dash lines. The model predictions are plotted using step lines.

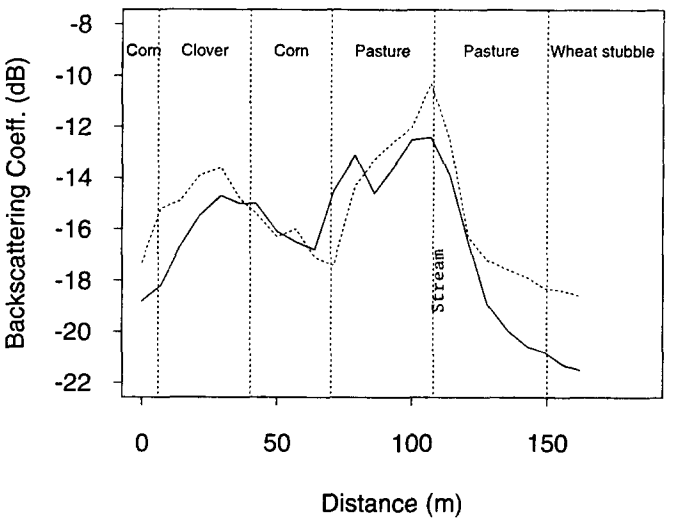

Figure 8. Temporal variations of the SAR signals along transects P_1 and P_2. Dash line represents data taken on 17 July 1990. Data taken on 10 July 1990 is plotted using solid line.

To examine how the SAR responds to temporal variation of soil moisture, we plot the SAR backscattering coefficients of 10 and 17 July 1990 in Figure 8. It is found that the sensitivity of the SAR echoes to the change in soil moisture varies with the land cover type. As indicated in the figure, the 10% soil moisture increase between 10 and 17 July has little effect on the SAR echoes over the corn field, while producing a 3-dB change over the wheat stubble and clover areas. A microwave backscattering model developed by Lang et al. (1986) is employed to investigate the cause behind the observed phenomenon. Radar backscattering processes over various types of vegetation canopies are simulated using the vegetation configurations collected over the fields. The simulation results indicate that, over the corn field, the vegetation volume scattering accounts for more than 55% of the L-band total radar backscatter, as opposed to under 15% for the wheat stubble and clover areas. Since the configurations of the corn field do not change much during the short period, it is understandable why there is a lack of sensitivity over the area. Although the predicted values may be model-dependent, the marked difference in the estimated percentages has left little doubt that the SAR echoes from various types of land cover are governed by different mechanisms. These results have an important implication on the development of the soil moisture inversion algorithm for the SAR. It suggests that, in order to accurately estimate the soil moisture content, one needs to filter out the portion of the echoes that are not directly associated with the soil moisture, especially under the situations where the vegetation volume contribution is important.

Another factor needed to be considered is the topography effect. Calculated from the geometry of the SAR system and the DEM-registered imagery, the averaged local incidence angle of the north bank (distance greater than 105 m) is approximately 10° less than that of the south bank. A similar aircraft campaign conducted 1 year later in Europe has showed that this 10° difference in local incidence angle can result in a change in the SAR echoes of several dBs in magnitude over pasture areas (Lin et al., 1993). In general, the effects of vegetation canopy and topography are entangled, making the interpretation of the SAR signals a difficult task. This is particularly the case for the small-scale analysis along transects because the speckle inherent in the SAR imagery, and the problems occurring in image processing and calibration may be important. Thus, the hypotheses presented above are subject to further verifications.

The soil moisture patterns predicted by the hydrologic model are consistent with one's expectations, that is, higher soil wetness for areas closer to the stream (see Figs. 7 and 8). This suggests that the hill-slope

processes are well represented by the hydrologic model. However, the distinct soil moisture variations between the near-stream pasture zone and the corn field are missing from the model's predictions, partly because of the size of the computational grid element used in simulation (i.e., 30 m × 30 m). To resolve the small scale soil moisture variations often occurring across zones with different vegetation cover, one needs to run the model on a grid resolution that is comparable to that of the SAR or the ground measurements, which will greatly increase the computational burden and data requirements. High resolution remote sensors such as the SAR might help in fullfilling this requirement, though many problems remain to be solved in the process.

Watershed Comparisons

Intercomparisons of the watershed averaged soil moisture estimates from various sources are conducted over the densely sampled WD38 subwatershed (see Fig. 1). The WD38 subwatershed has a drainage area of 50 ha and is nearly all cropped.

To estimate the watershed averaged soil moistures from the PBMR brightness temperatures, we apply the vegetation correction procedure, described in the subsection Passive Microwave Radiometer over three different types of land cover, namely, corn (38%), small grains (28%), and pasture and hay (27%). The values within the parentheses represent the percentage area of WD38 occupied by each category. Forest (6%) and residential area (1%) are excluded from computation because the measured brightness temperatures are not related to soil moisture under these conditions. The vegetation water content and the estimated optical thickness τ of each type of land cover are listed in Table 5, along with the watershed averaged optical thickness $\bar{\tau}$.

To extract soil moistures from the SAR data, we select an "optimal" empirical relationship from Table 4 for each type of land cover, considering both the sensitivity (i.e., slope) and the goodness-of-fit. The relationships chosen are listed as follows:

$$\mathbf{M}_v = \begin{cases} 64.454 + 4.915\bar{\sigma}^0_{cvv}, & \text{for corn,} \\ 87.214 + 3.481\bar{\sigma}^0_{Lvv}, & \text{for small grains,} \\ 95.083 + 5.161\bar{\sigma}^0_{Lvv}, & \text{for pasture and hay,} \end{cases} \quad (5)$$

Table 5. Vegetation Water Content and Estimated Optical Thickness for Each Type Land Cover for the WD38 Watershed

Land Cover	*Area Percentage (%)*	*Vegetation Water Content (kg/m²)*	*Optical Thickness*[a]
Corn	38	2.0	0.35
Small grains	28	0.4	0.15
Pasture and hay	27	0.1	0.10
Avg. $\bar{\tau}$ =	0.20		

[a] Estimated at wavelength = 21 cm.

where M_v is volumetric soil moisture content (%), $\bar{\sigma}^0_{cvv}$ and $\bar{\sigma}^0_{Lvv}$ are the field-averaged VV-polarized backscattering coefficients in dB for the C-band and L-band, respectively. Notice that multifrequency data are used here to improve the estimation accuracy. Despite the good fit in some cases (e.g., $\bar{\sigma}^0_{LHV}$ for corn), the HV-polarized signals are not employed because the calibration accuracy of the cross-polarized signals is usually inferior than that of the like-polarized signals. Figures 9a, 9b, and 9c display the estimated regression lines for corns, small grains, and pastures, respectively.

As mentioned earlier, in order to apply the above relationships over the WD38 watershed, it is necessary to check whether the field conditions of the watershed satisfy the range of validity of these empirical relationships. This is done by comparing the local incidence angles and vegetation properties of all fields within the WD38 watershed with the range of field conditions listed in Table 3. It is found that the majority of the fields within the WD38 watershed have an averaged local incidence angle between 35° and 45°, and have similar vegetation configurations as those of the verification sites. These results serve as a partial justification to the SAR inversion algorithm used in this study.

Following the verification study, Eq. (5) is applied to extract soil moistures from the SAR data on a field basis. Field averages are used to reduce the influences of the speckle and the bad pixels. The definition of the field boundary is derived from the georeferenced land cover map. As a rule of thumb, we try to include as many pixels within the field boundary as possible when computing the field averages. A field is excluded from computation if it contains less than 10 SAR pixels, or if it does not satisfy the range of validity of the empirical relationships. For such fields, their soil moisture contents will be interpolated from the surrounding estimates. Forest and residential areas are again excluded from analysis for the same reason described above.

Table 6 lists the watershed averaged soil moisture variations during the course of the experiment for the WD38 watershed, estimated from the two microwave sensors and the hydrologic model. Ground measurements taken within the WD38 watershed are averaged and listed for comparisons. The total number of ground samples is approximately 60 except on 15 July when only 33 were taken. It can be seen from the table that the watershed averaged soil moisture estimates from the two microwave remote sensors are in good agreement (within 15%) with the ground measurements despite the rather simple estimation procedures are used. These results, however, should not be overstated because part of the ground measurements have been used in deriving the inversion algorithms for the remote sensors.

It should be mentioned that, although the PBMR and the SAR yield similar soil moisture estimates over the WD38 watershed, the characteristics of these two

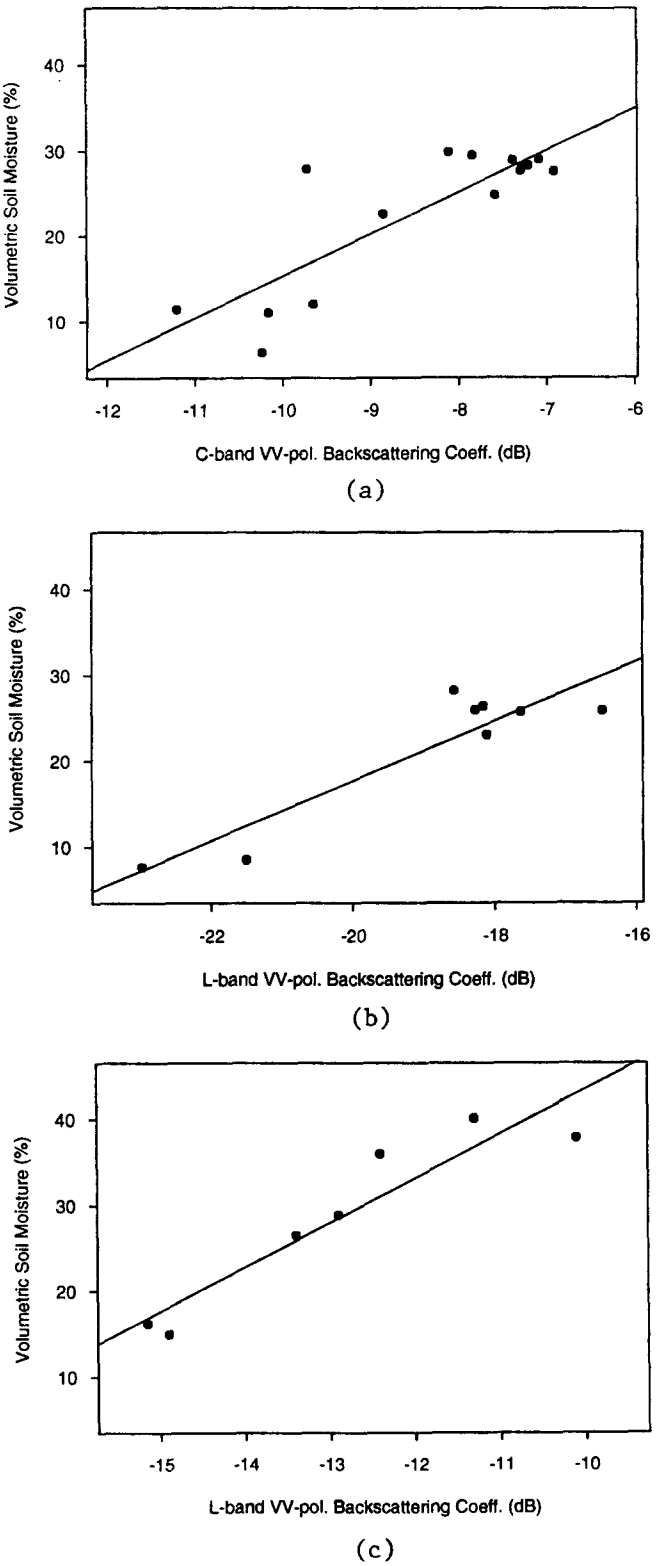

Figure 9. Regression relationships between the backscattering coefficients and the volumetric soil moisture contents for a) corns, b) small grains, and c) pastures.

measurements are actually quite different. The SAR measurements provide a better resolution than the PBMR, in spite of the reduced resolution through the use of the field averaged quantities in estimation. This kind of information can be very useful for studies that requires detailed spatial soil moisture distributions. It also has the potential to be the direct input to distributed hydrologic models. The major problem lies in the fact that, due to its sensitivity to topography and vegetation properties, a robust inversion algorithm for the SAR is still not available. On the contrary, the vegetation correction and the weighting procedures for the PBMR developed from previous experiments have been successfully applied to the heterogeneous WD38 watershed. The accuracy of the PBMR measurements are expected to improve with the scale and the homogeneity of the studied area. This feature has made the PBMR a good choice for studies in the regional scale where the approximate soil moisture pattern, instead of the detailed spatial distribution, may suffice for the purposes. Therefore, the decision of which instruments should be used depends on the data resolution required for the intended applications, as well as the available information regarding the target area.

Estimates from the hydrologic model are wetter than other measurements. The temporal variation, however, reflects the weather conditions. The discrepancy between the model predictions and the ground measurements may be caused by errors in the initial soil moisture conditions. The initialization of the hydrologic model is performed using observed precipitation and stream discharge. In applying the model to an experiment such as MAC-HYDRO'90, two fundamental difficulties arise that can affect the model's performance. The major difficulty occurs during the summer season when the upper soil layer effectively becomes disconnected with the lower portion of the soil column (i.e., the saturated portion of the column), which is draining and providing the observed base discharge in the stream. Essentially no vertical percolation is occurring. Thus the standard initialization procedure provides limited information about the state of the surface soil moisture. The second

Table 6. Averaged Volumetric Soil Moisture Estimates for the WD38 Subwatershed

Date	*PBMR (%)*	*SAR (%)*	*Model (%)*	*Ground (%)*
10 July	13	14.5	28	12.0
13 July	–	22.9	38	25.1
15 July	23	24.0	36	25.0
17 July	26	25.1	33	22.8
18 July	19	–	32	20.8
19 July	19	–	30	19.7
20 July	–	–	26	17.5

difficulty is related to the first and is concerned with the short duration of the experiment. The initial conditions persist until a sequence of storm and interstorm periods perturb the catchment sufficiently so that the water fluxes (infiltration and evaporation) and soil moisture represent the modeled processes. For MAC-HYDRO'90, errors in the model initialization still persisted throughout the 11-day simulation period. In the case of the results shown in Table 6, the soil moisture observations were not used to help initialize the hydrologic model. Therefore, errors in this variable, due to the above reasons, can be expected.

Having recognized the problems incurred by using the conventional calibration scheme, we next explore the usage of the remotely sensed soil moistures as a feedback to correct the initial state of the hydrologic model. Figure 10 summarizes the preliminary results by showing the watershed-averaged soil moisture temporal variation of a new simulation. This simulation is based upon a different initial condition derived from matching the model simulated soil moisture with the PBMR estimated value on 10 July 1990, that is, the second day of the simulation. As indicated in the figure, the model simulated soil moisture pattern is in good agreement with other measurements. These results underscore the potential of the remote sensing technique in application to hydrologic modeling. However, a number of problems need to be studied in order to efficiently and appropriately utilize these information:

1. The new simulation has produced less runoff than observed records. This is resulted from the drier initial soil moisture condition derived from the PBMR measurements. How to simultaneously reproduce the variations of the runoff and the soil moisture pattern, as well as other hydrologic fluxes, remains to be an unanswered question.
2. The new simulation has only utilized the 10 July PBMR measurement in a rather simple fashion. There is a need to find an appropriate way to incorporate the multitemporal remotely sensed data and to take into consideration of the different features provided by the two sensors. In principle, temporal changes between scenes can help to identify areas that have undergone large soil moisture variations. These areas are likely to represent the hydrologically active areas. If the hydrologic model's soil moisture distribution over these active areas can be routinely updated, the accuracy of the model's predictions should improve.
3. The above simulation is conducted over a small heterogeneous watershed located in a temperate humid area. One should evaluate whether the above results are still effective should the site of the simulation be located in a different climate regime and / or over a larger watershed characterized by different types of land cover.

Figure 10. Temporal variation of model simulated soil moistures over the WD38 watershed using a PBMR-derived initial condition. PBMR estimates are represented by open circles, SAR estimates by triangles, and ground measurements by + s.

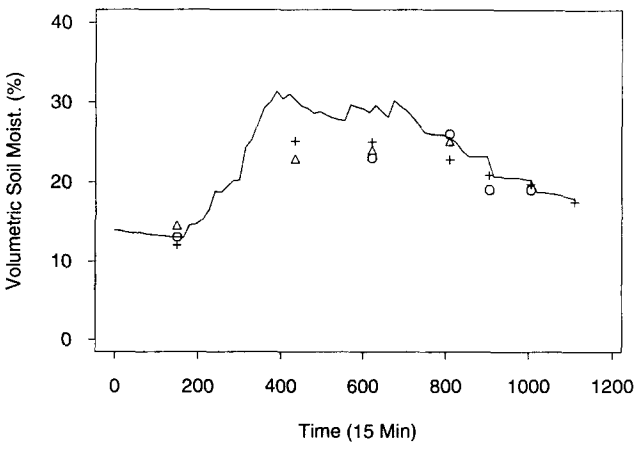

CONCLUSIONS

Soil moisture estimates from two airborne microwave sensors are compared with model simulated results and ground measurements over an agricultural watershed located in central Pennsylvania. Results can be summarized as follows:

1. Both microwave sensors successfully reflected the temporal variation of soil moisture over the verification site.
2. Prediction from the hydrologic model and the SAR signals have displayed anticipated soil moisture patterns along transects. However, the apparent soil moisture variations between the near-stream pasture area and the corn field have not been detected by either technique.
3. Watershed averaged soil moisture estimates from both microwave sensors are in good agreement with the ground measurements. Estimates from the hydrologic model calibrated by using the streamflow records appear to be too wet. However, the model has predicted the temporal soil moisture variations correctly. Remotely sensed soil moisture data have the potential to be used as a feedback to correct the model's initial condition.
4. The PBMR estimation procedure developed from previous experiments has yielded satisfactory results. Its resolution is limited by the current georeferencing technique. The SAR provides a more detailed spatial soil moisture distribution. However, the inversion algorithm for the SAR is still

site-specific. The choice of the appropriate instrument depends on the intended applications and the available information regarding the target area.

The authors thank D. J. Thongs for help in image processing. This study was supported by NASA Global Change Graduate Fellowship (NGT-30049), NASA Grant NAG5-1628, and USDA Cooperative Agreement 58-3K47-0-039 for application of SIR-C Synthetic Aperture Radar to Hydrology. Support from NASA and USDA is highly appreciated.

REFERENCES

Beven, K. (1983), Surface Water Hydrology-Runoff Generation and Basin Structure, *Rev. Geophysics and Space Physics*, Vol. 21, pp. 721–730.

Dobson, M. C., Ulaby, F. T., Hallikasnen, M, and El-Rayes, M. (1985), Microwave dielectic behavior of wet soil—Part II: Dielectric mixing models, *IEEE Trans. Geosci. Remote Sens.* GE-23:35–46.

Durden, S. L., Klein, J. D., and Zebker, H. A. (1991), Polarimetric radar measurements of a forested area near Mt. Shasta, *IEEE Trans. Geosci. Remote Sens.* 29:444–450.

Engman, E. T. (1990), Progress in microwave remote sensing of soil moisture, Can. *J. Remote Sens.* 16:6–14.

Held, D. N., et al. (1988), the NASA / JPL Multifrequency, Multipolarization Airborne SAR System, in *Proc. IGARSS'88*, Edinburgh, Scotland, pp. 317–322.

Jackson, T. J., and Schmugge, T. J. (1991), Vegetation effects on the microwave emission of soils, *Remote Sens. Environ.* 36:203–212.

Jackson, T. J., Hawley, M. E., and O'Neill, P. E. (1987), Preplanting soil moisture using passive microwave sensors, *Water Resour. Bull.* 23:11–19.

Lang, R. H., Saatchi, S., and LeVine, D. M. (1986), Microwave backscattering from an anisotropic soybean canopy, in *Proc. IGARSS'86*, Zurich.

Lin, D.-S., Wood, E. F., Saatchi, S., and Beven, K. (1993), Soil moisture estimation during MAC-EUROPE'91 using AIRSAR, in *Proc. 25th Int. Symp. Remote Sens. Global Environ. Change*, Graz, Austria.

League, K. M., and Freeze, R. A. (1985), A comparison of rainfall-runoff modeling techniques on small upland catchments, *Water Resour. Res.* 21:229–248.

Oh, Y., Sarabandi, K., and Ulaby, F. T. (1992), An empirical model and an inversion techniques for radar scattering for bare soil surfaces, *IEEE Trans. Geosci. Remote Sens.* 30: 370–381.

Paniconi, C., and Wood, E. F. (1993), A detailed model for simulation of catchment scale subsurface hydrologic processes, *Water Resours. Res.*, 29:1601–1620.

Paniconi, C., Aldama, A. A., and Wood, E. F. (1991), Numerical evaluation of iterative and noniterative methods for the solution of the nonlinear Richards equation, *Water Resours. Res.* 27:1114–1163.

Pultz, T. J., Leconte, R, Brown, R. J., and Brisco, B. (1990), Quantitative soil moisture extraction from airborne SAR data, *Can. J. Remote Sens.* 16:56–62.

Rogowski, A. S., Engman, E. T., and Jacoby, E. L. (1974), Transient response of a layered, sloping soil to natural rainfall in the presence of a shallow water table, USDA, ARS Report ARS-NE-30, Hyattsville, MD.

Soares, J. V., Shi, J. C., Hess, L., Engman, E. T., and van Zyl, J. J. (1991), Estimation of bare soil evaporation from a multi-frequency airborne SAR, in *24th Int. Symp. Remote Sens. Environ.*, Rio de Janeiro, Brazil.

Schmugge, T. J., Wang, J. R., and Asrar, G. (1988), Results from the push broom microwave radiometer flights over the Konza Prairie in 1985, *IEEE Trans. Geosci. Remote Sens.* 26:590–596.

Schmugge, T. J., Jackson, T. J., Kustas, W. P., and Wang, J. R. (1992), Passive microwave remote sensing of soil moisture: results from HAPEX, FIFE and MONSOON'90. *Photogramm. Eng. Remote Sens.*, forthcoming.

Troch, P. A., Mancini, M., Paniconi, C., and Wood, E. F. (1993), Evaluation of a distributed catchment scale water balance model, *Water Resours. Res.*, 29:1805–1817.

van Genuchten, M. T., and Nielsen, D. R. (1985), On describing and predicting the hydraulic properties of unsaturated soils, *Ann. Geophys.* 3:615–628.

van Zyl, J., Burnette, C. F., Zebker, H. A., Freeman, A., and Holt, J. (1990), *POLCAL User's manual*, Jet Propulsion Lab., Cal. Tech., Pasadena, CA.

Wood, E. F. (1991), Global scale hydrology: advances in land surface modeling, *Rev. Geophys. Suppl.* 193–201.